Beyond 2000 in Computational Geotechnics – 10 Years of PLAXIS © 1999 Balkema, Rotterdam, ISBN 90 5809 040 X

The hardening soil model: Formulation and verification

T. Schanz
Laboratory of Soil Mechanics, Bauhaus-University Weimar, Germany
P.A. Vermeer
Institute of Geotechnical Engineering, University Stuttgart, Germany
P.G. Bonnier
PLAXIS B.V., Netherlands

Keywords: constitutive modeling, HS-model, calibration, verification

ABSTRACT: A new constitutive model is introduced which is formulated in the framework of classical theory of plasticity. In the model the total strains are calculated using a stress-dependent stiffness, different for both virgin loading and un-/reloading. The plastic strains are calculated by introducing a multi-surface yield criterion. Hardening is assumed to be isotropic depending on both the plastic shear and volumetric strain. For the frictional hardening a non-associated and for the cap hardening an associated flow rule is assumed.

First the model is written in its rate form. Therefor the essential equations for the stiffness modules, the yield-, failure- and plastic potential surfaces are given.

In the next part some remarks are given on the models incremental implementation in the PLAXIS computer code. The parameters used in the model are summarized, their physical interpretation and determination are explained in detail.

The model is calibrated for a loose sand for which a lot of experimental data is available. With the so calibrated model undrained shear tests and pressuremeter tests are back-calculated.

The paper ends with some remarks on the limitations of the model and an outlook on further developments.

1 INTRODUCTION

Due to the considerable expense of soil testing, good quality input data for stress-strain relationships tend to be very limited. In many cases of daily geotechnical engineering one has good data on strength parameters but little or no data on stiffness parameters. In such a situation, it is no help to employ complex stress-strain models for calculating geotechnical boundary value problems. Instead of using Hooke's single-stiffness model with linear elasticity in combination with an ideal plasticity according to Mohr-Coulomb a new constitutive formulation using a double-stiffness model for elasticity in combination with isotropic strain hardening is presented.

Summarizing the existing double-stiffness models the most dominant type of model is the Cam-Clay model (Hashiguchi 1985, Hashiguchi 1993). To describe the non-linear stress-strain behaviour of soils, beside the Cam-Clay model the pseudo-elastic (hypo-elastic) type of model has been developed. There an Hookean relationship is assumed between increments of stress and strain and non-linearity is achieved by means of varying Young's modulus. By far the best known model of this category ist the Duncan-Chang model, also known as the hyperbolic model (Duncan & Chang 1970). This model captures soil behaviour in a very tractable manner on the basis of only two stiffness parameters and is very much appreciated among consulting geotechnical engineers. The major inconsistency of this type of model which is the reason why it is not accepted by scientists is that, in contrast to the elasto-plastic type of model, a purely hypo-elastic model cannot consistently distinguish between loading and unloading. In addition, the model is not suitable for collapse load computations in the fully plastic range.

These restrictions will be overcome by formulating a model in an elasto-plastic framework in this paper. Doing so the Hardening-Soil model, however, supersedes the Duncan-Chang model by far. Firstly by using the theory of plasticity rather than the theory of elasticity. Secondly by including soil dilatancy and thirdly by introducing a yield cap.

In contrast to an elastic perfectly-plastic model, the yield surface of the Hardening Soil model is not fixed in principal stress space, but it can expand due to plastic straining. Distinction is made between two main types of hardening, namely shear hardening and compression hardening. Shear hardening is used to model irreversible strains due to primary deviatoric loading. Compression hardening is used to model irreversible plastic strains due to primary compression in oedometer loading and isotropic loading.

For the sake of convenience, restriction is made in the following sections to triaxial loading conditions with $\sigma_2' = \sigma_3'$ and σ_1' being the effective major compressive stress.

2 CONSTITUTIVE EQUATIONS FOR STANDARD DRAINED TRIAXIAL TEST

A basic idea for the formulation of the Hardening-Soil model is the hyperbolic relationship between the vertical strain ε_1, and the deviatoric stress, q, in primary triaxial loading. When subjected to primary deviatoric loading, soil shows a decreasing stiffness and simultaneously irreversible plastic strains develop. In the special case of a drained triaxial test, the observed relationship between the axial strain and the deviatoric stress can be well approximated by a hyperbola (Kondner & Zelasko 1963). Standard drained triaxial tests tend to yield curves that can be described by:

$$\varepsilon_1 = \frac{q_a}{2E_{50}} \frac{(\sigma_1 - \sigma_3)}{q_a - (\sigma_1 - \sigma_3)} \quad \text{for} \quad q < q_f \quad . \tag{1}$$

The ultimate deviatoric stress, q_f, and the quantity q_a in Eq. 1 are defined as:

$$q_f = \frac{6 \sin \varphi_p}{3 - \sin \varphi_p} (p + c \cot \varphi_p) \qquad q_a = \frac{q_f}{R_f} \quad . \tag{2}$$

The above relationship for q_f is derived from the Mohr-Coulomb failure criterion, which involves the strength parameters c and φ_p. As soon as $q = q_f$, the failure criterion is satisfied and perfectly plastic yielding occurs. The ratio between q_f and q_a is given by the failure ratio R_f, which should obviously be smaller than 1. $R_f = 0.9$ often is a suitable default setting. This hyperbolic relationship is plotted in Fig. 1.

2.1 *Stiffness for primary loading*

The stress strain behaviour for primary loading is highly nonlinear. The parameter E_{50} is the confining stress dependent stiffness modulus for primary loading. E_{50} is used instead of the initial modulus E_i for small strain which, as a tangent modulus, is more difficult to determine experimentally. It is given by the equation:

$$E_{50} = E_{50}^{ref} \left(\frac{\sigma_3 + c \cot \varphi_p}{\sigma^{ref} + c \cot \varphi_p} \right)^m \quad . \tag{3}$$

E_{50}^{ref} is a reference stiffness modulus corresponding to the reference stress p^{ref}. The actual stiffness depends on the minor principal stress, σ_3', which is the effective confining pressure in a triaxial test. The amount of stress dependency is given by the power m. In order to simulate a logarithmic stress dependency, as observed for soft clays, the power should be taken equal to 1.0. As a

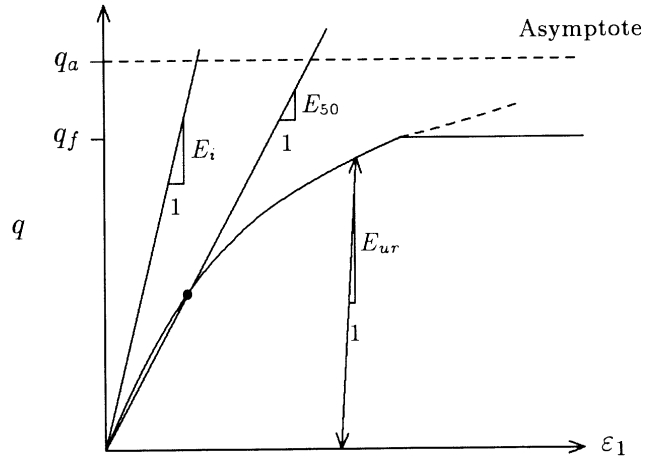

Figure 1. Hyperbolic stress-strain relation in primary loading for a standard drained triaxial test.

secant modulus E_{50}^{ref} is determined from a triaxial stress-strain-curve for a mobilization of 50% of the maximum shear strength q_f.

2.2 *Stiffness for un-/reloading*

For unloading and reloading stress paths, another stress-dependent stiffness modulus is used:

$$E_{ur} = E_{ur}^{ref} \left(\frac{\sigma_3 + c\cot\varphi_p}{\sigma^{ref} + c\cot\varphi_p} \right)^m \quad , \tag{4}$$

where E_{ur}^{ref} is the reference Young's modulus for unloading and reloading, corresponding to the reference pressure σ^{ref}. Doing so the un-/reloading path is modeled as purely (non-linear) elastic. The elastic components of strain ε^e are calculated according to a Hookean type of elastic relation using Eqs. 4 + 5 and a constant value for the un-/reloading Poisson's ratio υ_{ur}.

$$G_{ur} = \frac{1}{2(1+\nu_{ur})} E_{ur} \quad , \qquad \sigma^{ref} = 100\,kPa \quad . \tag{5}$$

For drained triaxial test stress paths with $\sigma_2 = \sigma_3 =$ constant, the elastic Young's modulus E_{ur} remains constant and the elastic strains are given by the equations:

$$\varepsilon_1^e = \frac{q}{E_{ur}} \quad , \qquad \varepsilon_2^e = \varepsilon_3^e = \nu_{ur} \frac{q}{E_{ur}} \quad . \tag{6}$$

Here it should be realised that restriction is made to strains that develop during deviatoric loading, whilst the strains that develop during the very first stage of the test are not considered. For the first stage of isotropic compression (with consolidation), the Hardening-Soil model predicts fully elastic volume changes according to Hooke's law, but these strains are not included in Eq. 6.

2.3 *Yield surface, failure condition, hardening law*

For the triaxial case the two yield functions f_{12} and f_{13} are defined according to Eqs. 7 and 8. Here

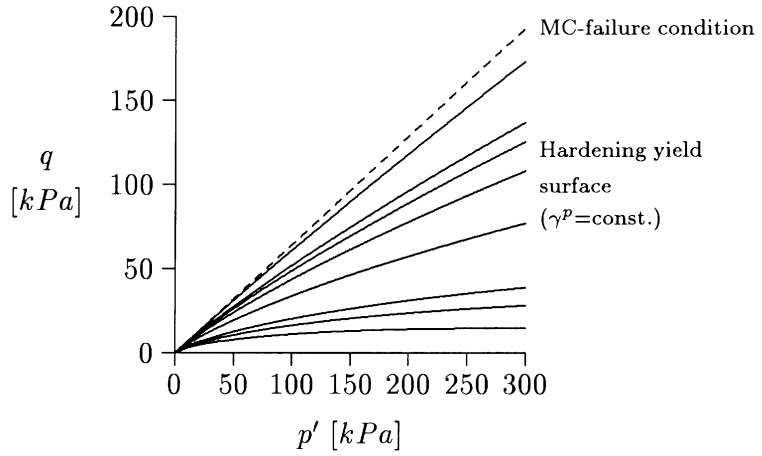

Figure 2. Successive yield loci for various values of the hardening parameter γ^p and failure surface.

the measure of the plastic shear strain γ^p according to Eq. 9 is used as the relevant parameter for the frictional hardening:

$$f_{12} = \frac{q_a}{E_{50}} \frac{(\sigma_1 - \sigma_2)}{q_a - (\sigma_1 - \sigma_2)} - \frac{2(\sigma_1 - \sigma_2)}{E_{ur}} - \gamma^p \quad , \tag{7}$$

$$f_{13} = \frac{q_a}{E_{50}} \frac{(\sigma_1 - \sigma_3)}{q_a - (\sigma_1 - \sigma_3)} - \frac{2(\sigma_1 - \sigma_3)}{E_{ur}} - \gamma^p \tag{8}$$

with the definition

$$\gamma^p := \varepsilon_1^p - \varepsilon_2^p - \varepsilon_3^p = 2\varepsilon_1^p - \varepsilon_v^p \approx 2\varepsilon_1^p \quad . \tag{9}$$

In reality, plastic volumetric strains ε_v^p will never be precisely equal to zero, but for hard soils plastic volume changes tend to be small when compared with the axial strain, so that the approximation in Eq. 9 will generally be accurate.

For a given constant value of the hardening parameter, γ^p, the yield condition $f_{12} = f_{13} = 0$ can be visualised in p'-q-plane by means of a yield locus. When plotting such yield loci, one has to use Eqs. 7 and 8 as well as Eqs. 3 and 4 for E_{50} and E_{ur} respectively. Because of the latter expressions, the shape of the yield loci depends on the exponent m. For m = 1.0 straight lines are obtained, but slightly curved yield loci correspond to lower values of the exponent. Fig. 2 shows the shape of successive yield loci for m = 0.5, being typical for hard soils. For increasing loading the failure surfaces approach the linear failure condition according to Eq. 2.

2.4 *Flow rule, plastic potential functions*

Having presented a relationship for the plastic shear strain, γ^p, attention is now focused on the plastic volumetric strain ε_v^p. As for all plasticity models, the Hardening-Soil model involves a relationship between rates of plastic strain, i.e. a relationship between $\dot{\varepsilon}_v^p$ and $\dot{\gamma}^p$. This flow rule has the linear form:

$$\dot{\varepsilon}_v^p = \sin\psi_m \, \dot{\gamma}^p \quad . \tag{10}$$

Clearly, further detail is needed by specifying the mobilized dilatancy angle ψ_m. For the present model, the expression:

$$\sin\psi_m = \frac{\sin\varphi_m - \sin\varphi_{cv}}{1 - \sin\varphi_m \sin\varphi_{cv}} \tag{11}$$

is adopted, where φ_{cv} is the critical state friction angle, being a material constant independent of density (Schanz & Vermeer 1996), and φ_m is the mobilized friction angle:

$$\sin\varphi_m = \frac{\sigma_1 - \sigma_3}{\sigma_1 + \sigma_3 - 2c\cot\varphi_p} \quad . \tag{12}$$

The above equations correspond to the well-known stress-dilatancy theory (Rowe 1962, Rowe 1971), as explained by (Schanz & Vermeer 1996). The essential property of the stress-dilatancy theory is that the material contracts for small stress ratios $\varphi_m < \varphi_{cv}$, whilst dilatancy occurs for high stress ratios $\varphi_m < \varphi_{cv}$. At failure, when the mobilized friction angle equals the failure angle, φ_p, it is found from Eq. 11 that:

$$\sin\psi_{cv} = \frac{\sin\varphi_p - \sin\psi_p}{1 - \sin\varphi_p \sin\psi_p} \quad . \tag{13}$$

Hence, the critical state angle can be computed from the failure angles φ_p and ψ_p. The above definition of the flow rule is equivalent to the definition of definition of the plastic potential functions g_{12} and g_{13} according to:

$$\begin{aligned} g_{12} &= (\sigma_1 - \sigma_2)/2 - (\sigma_1 + \sigma_2)/2 \cdot \sin\psi_m \quad , \\ g_{13} &= (\sigma_1 - \sigma_3)/2 - (\sigma_1 + \sigma_3)/2 \cdot \sin\psi_m \quad . \end{aligned} \tag{14}$$

Using the *Koiter-rule* (Koiter 1960) for yielding depending on two yield surfaces (*Multi-surface plasticity*) one finds:

$$\dot{\varepsilon}^p = \dot{\Lambda}_{12}\frac{\partial g_{12}}{\partial \boldsymbol{\sigma}} + \dot{\Lambda}_{13}\frac{\partial g_{13}}{\partial \boldsymbol{\sigma}} = \dot{\Lambda}_{12}\begin{bmatrix} \frac{1}{2} - \frac{1}{2}\sin\psi \\ -\frac{1}{2} - \frac{1}{2}\sin\psi \\ 0 \end{bmatrix} + \dot{\Lambda}_{13}\begin{bmatrix} \frac{1}{2} - \frac{1}{2}\sin\psi \\ 0 \\ -\frac{1}{2} - \frac{1}{2}\sin\psi \end{bmatrix} \tag{15}$$

Calculating the different plastic strain rates by this equation, Eq. 10 directly follows.

3 TIME INTEGRATION

The model as described above has been implemented in the finite element code PLAXIS (Vermeer & Brinkgreve 1998). To do so, the model equations have to be written in incremental form. Due to this incremental formulation several assumptions and modifications have to be made, which will be explained in this section.

During the global iteration process, the displacement increment follows from subsequent solution of the global system of equations:

$$\boldsymbol{K}\,\Delta\boldsymbol{u} = \Delta\boldsymbol{f}_{ext} - \Delta\boldsymbol{f}_{int} \quad , \tag{16}$$

where $\boldsymbol{K}$ is the global stiffness matrix in which we use the elastic Hooke's matrix $\boldsymbol{D}$, $\boldsymbol{f}_{ext}$ is a global load vector following from the external loads and $\boldsymbol{f}_{int}$ is the global reaction vector following from the stresses. The stress at the end of an increment σ^1 can be calculated (for a given strain increment $\Delta\varepsilon$) as:

$$\boldsymbol{\sigma}^1 = \boldsymbol{\sigma}^0 + \Delta\boldsymbol{\sigma} \quad , \tag{17}$$

$$\Delta\boldsymbol{\sigma} = \overset{4}{\mathbf{D}} \left(\Delta\boldsymbol{\varepsilon} - \Delta\Lambda \frac{\partial g}{\partial \boldsymbol{\sigma}} \right) \quad , \tag{18}$$

$$\gamma^p = \gamma_0^p + \Delta\gamma^p \tag{19}$$

where

σ^0 , stress at the start of the increment,

$\Delta\sigma$, resulting stress increment,

$\overset{4}{\mathbf{D}}$, Hooke's elasticity matrix, based on the unloading-reloading stiffness,

$\Delta\varepsilon$, strain increment (= $B\Delta u$),

γ^p , measure of the plastic shear strain, used as hardening parameter,

$\Delta\Lambda$, increment of the non-negative multiplier,

g , plastic potential function.

The multiplier Λ has to be determined from the condition that the function $f(\sigma^1, \gamma^p) = 0$ has to be zero for the new stress and deformation state.

As during the increment of strain the stresses change, the stress dependant variables, like the elasticity matrix and the plastic potential function g, also change. The change in the stiffness during the increment is not very important as in many cases the deformations are dominated by plasticity.

This is also the reason why a Hooke's matrix is used. We use the stiffness matrix $\overset{4}{\mathbf{D}}$ based on the stresses at the beginning of the step (*Euler explicit*). In cases where the stress increment follows from elasticity alone, such as in unloading or reloading, we iterate on the average stiffness during the increment.

The plastic potential function g also depends on the stresses and the mobilized dilation angle ψ_m. The dilation angle for these derivatives is taken at the beginning of the step. The implementation uses an implicit scheme for the derivatives of the plastic potential function g. The derivatives are taken at a predictor stress σ^{tr}, following from elasticity and the plastic deformation in the previous iteration:

$$\boldsymbol{\sigma}^{tr} = \boldsymbol{\sigma}^0 + \overset{4}{\mathbf{D}}\, \Delta\boldsymbol{\varepsilon} \quad . \tag{20}$$

The calculation of the stress increment can be performed in principal stress space. Therefore initially the principal stresses and principal directions have to be calculated from the Cartesian stresses, based on the elastic prediction. To indicate this we use the subscripts 1, 2 and 3 and have $\sigma_1 \geq \sigma_2 \geq \sigma_3$ where compression is assumed to be positive.

Principal plastic strain increments are now calculated and finally the Cartesian stresses have to be back-calculated from the resulting principal constitutive stresses. The calculation of the constitutive stresses can be written as:

$$\boldsymbol{\sigma}^1 = \boldsymbol{\sigma}^{tr} - \Delta\Lambda\mathbf{b} \qquad \text{with} \qquad \mathbf{b} = \overset{4}{\mathbf{D}} \frac{\partial g}{\partial \boldsymbol{\sigma}} \quad . \tag{21}$$

From this the deviatoric stress q ($\sigma_1 - \sigma_3$) and the asymptotic deviatoric stress q_a can be expressed in the elastic prediction stresses and the multiplier $\Delta\Lambda$:

$$q = \sigma_1^{tr} - \sigma_3^{tr} - \Delta\Lambda(b_1 - b_3) = q^{tr} - \Delta\Lambda(b_1 - b_3) \ , \tag{22}$$

$$q_a = \frac{2\sin\varphi}{1-\sin\varphi}\frac{1}{R_f}\sigma_3^*$$

$$= \frac{2\sin\varphi}{1-\sin\varphi}\frac{1}{R_f}(\sigma_3^{*tr} - \Delta\Lambda b_3) \quad , \tag{23}$$

where

$$\sigma_3^* = (\sigma_3 + c\cot\varphi) \quad . \tag{24}$$

For these stresses the function

$$f(\boldsymbol{\sigma}^1) - f(\boldsymbol{\sigma}^0) - \Delta\gamma^p = 0 \tag{25}$$

should be zero. As the increment of the plastic shear strain $\Delta\gamma^p$ also depends linearly on the multiplier $\Delta\Lambda$, the above formulae result in a (complicated) quadratic equation for the multiplier $\Delta\Lambda$ which can be solved easily. Using the resulting value of $\Delta\Lambda$, one can calculate (incremental) stresses and the (increment of the) plastic shear strain.

In the above formulation it is assumed that there is a single yield function. In case of triaxial compression or triaxial extension states of stress there are two yield functions and two plastic potential functions. Following (Koiter 1960) one can write:

$$\boldsymbol{\sigma}^1 = \boldsymbol{\sigma}^{tr} - \Delta\Lambda_{12}\overset{4}{\mathbf{D}}\frac{\partial g_{12}}{\partial\boldsymbol{\sigma}} - \Delta\Lambda_{13}\overset{4}{\mathbf{D}}\frac{\partial g_{13}}{\partial\boldsymbol{\sigma}} \quad , \tag{26}$$

where the subscripts indicate the principal stresses used for the yield and potential functions. At most two of the multipliers are positive. In case of triaxial compression we have $\sigma_2 = \sigma_3$, $\Lambda_{23} = 0$ and we use two consistency conditions instead of one as above. The increment of the plastic shear strain has to be expressed in the multipliers. This again results in a quadratic equation in one of the multipliers.

When the stresses are calculated one still has to check if the stress state violates the yield criterion $q \le q_f$. When this happens the stresses have to be returned to the Mohr-Coulomb yield surface.

4 ON THE CAP YIELD SURFACE

Shear yield surfaces as indicated in Fig. 2 do not explain the plastic volume strain that is measured in isotropic compression. A second type of yield surface must therefore be introduced to close the elastic region in the direction of the p-axis. Without such a cap type yield surface it would not be possible to formulate a model with independent input of both E_{50} and E_{oed}. The triaxial modulus largely controls the shear yield surface and the oedometer modulus controls the cap yield surface. In fact, E_{50}^{ref} largely controls the magnitude of the plastic strains that are associated with the shear yield surface. Similarly, E_{oed}^{ref} is used to control the magnitude of plastic strains that originate from the yield cap. In this section the yield cap will be described in full detail. To this end we consider the definition of the cap yield surface ($a = c\cot\varphi$):

$$f_c = \frac{\tilde{q}^2}{M^2} + (p+a)^2 - p_c + a)^2 \ , \tag{27}$$

where M is an auxiliary model parameter that relates to K_0^{NC} as will be discussed later. Further more we have $p = (\sigma_1 + \sigma_2 + \sigma_3)$ and

$$\tilde{q} = \sigma_1 + (\alpha - 1)\sigma_2 - \alpha\sigma_3 \ , \tag{28}$$

with

$$\alpha = \frac{3 + \sin\varphi}{3 - \sin\varphi} \ . \tag{29}$$

q is a special stress measure for deviatoric stresses. In the special case of triaxial compression it yields $q = (\sigma_1 - \sigma_3)$ and for triaxial extension reduces to $q = \alpha\,(\sigma_1 - \sigma_3)$. For yielding on the cap surface we use an associated flow rule with the definition of the plastic potential g_c:

$$g_c = f_c \ . \tag{30}$$

The magnitude of the yield cap is determined by the isotropic pre-consolidation stress p_c. For the case of isotropic compression the evolution of p_c can be related to the plastic volumetric strain rate $\dot{\varepsilon}_v^p$:

$$\dot{\varepsilon}_v^p = \frac{\dot{p}}{K_c} - \frac{\dot{p}}{K_s} = \frac{1}{H}\dot{p} \ . \tag{31}$$

Here H is the *hardening modulus* according to Eq. 32, which expresses the relation between the elastic swelling modulus K_s and the elasto-plastic compression modulus K_c for isotropic compression:

$$H = \frac{K_c}{K_s - K_c} K_s \ . \tag{32}$$

From this definition follows a stress dependency of H. For the case of isotropic compression we have $q = 0$ and therefor $\dot{p} = \dot{p}_c$. For this reason we find Eq. 33 directly from Eq. 31:

$$\dot{p}_c = H\,\dot{\varepsilon}_v^p = H\,\dot{\Lambda}_c \frac{\partial g_c}{\partial p} = 2\,H\,\dot{\Lambda}_c\,p \ . \tag{33}$$

The plastic multiplier $\dot{\Lambda}_c$ referring to the cap is determined according to Eq. 35 using the additional consistency condition:

$$\dot{f}_c = \frac{\partial f_c}{\partial \boldsymbol{\sigma}} \cdot \dot{\boldsymbol{\sigma}} + \frac{\partial f_c}{\partial p_c}\dot{p}_c = 0 \tag{34}$$

$$\dot{\Lambda}_c = \frac{H}{2(p+a)} \left(\frac{p_c + a}{\sigma^{ref} + a} \right)^m \frac{\dot{p}_c}{\sigma^{ref} + a} \tag{35}$$

Using Eqs. 33 and 35 we find the hardening law relating p_c to the volumetric cap strain ε_v^c:

$$\varepsilon_v^c = \frac{H}{m+1} \left(\frac{p_c}{\sigma^{ref}} \right)^{m+1} \tag{36}$$

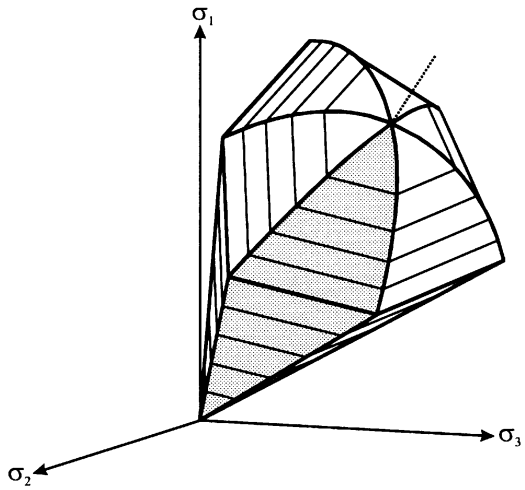

Figure 3. Representation of total yield contour of the Hardening-Soil model in principal stress space for cohesionless soil.

The volumetric cap strain is the plastic volumetric strain in isotropic compression. In addition to the well known constants *m* and σ_{ref} there is another model constant *H*. Both *H* and *M* are cap parameters, but they are not used as direct input parameters. Instead, we have relationships of the form $K_0^{NC} = K_0^{NC}$ (..., *M*, *H*) and $E_{oed}^{ref} = E_{oed}^{ref}$ (..., *M*, *H*), such that K_0^{NC} and E_{oed}^{ref} can be used as input parameters that determine the magnitude of *M* and *H* respectively. The shape of the yield cap is an ellipse in p – $\tilde{q}$ -plane. This ellipse has length $p_c + a$ on the *p*-axis and *M* ($p_c + a$) on the $\tilde{q}$ -axis. Hence, p_c determines its magnitude and *M* its aspect ratio. High values of *M* lead to steep caps underneath the Mohr-Coulomb line, whereas small *M*-values define caps that are much more pointed around the *p*-axis.

For understanding the yield surfaces in full detail, one should consider Fig. 3 which depicts yield surfaces in principal stress space. Both the shear locus and the yield cap have the hexagonal shape of the classical Mohr-Coulomb failure criterion. In fact, the shear yield locus can expand up to the ultimate Mohr-Coulomb failure surface. The cap yield surface expands as a function of the pre-consolidation stress p_c.

5 PARAMETERS OF THE HARDENING-SOIL MODEL

Some parameters of the present hardening model coincide with those of the classical non-hardening Mohr-Coulomb model. These are the failure parameters φ_p,, *c* and ψ_p. Additionally we use the basic parameters for the soil stiffness:

E_{50}^{ref} , secant stiffness in standard drained triaxial test,

E_{oed}^{ref} , tangent stiffness for primary oedometer loading and

m, power for stress-level dependency of stiffness.

This set of parameters is completed by the following advanced parameters:

E_{ur}^{ref} , unloading/ reloading stiffness,

v_{ur} , Poisson's ratio for unloading-reloading,

p^{ref}, reference stress for stiffnesses,

K_0^{NC} , K_0-value for normal consolidation and

R_f, failure ratio q_f / q_a.

Experimental data on m, E_{50} and E_{oed} for granular soils is given in (Schanz & Vermeer 1998).

5.1 *Basic parameters for stiffness*

The advantage of the Hardening-Soil model over the Mohr-Coulomb model is not only the use of a hyperbolic stress-strain curve instead of a bi-linear curve, but also the control of stress level dependency. For real soils the different modules of stiffness depends on the stress level. With the Hardening-Soil model a stiffness modulus E_{50}^{ref} is defined for a reference minor principal stress of $\sigma_3 = \sigma^{ref}$. As some readers are familiar with the input of shear modules rather than the above stiffness modules, shear modules will now be discussed. Within Hooke's theory of elasticity conversion between E and G goes by the equation $E = 2\,(1 + \nu)\,G$. As E_{ur} is a real elastic stiffness, one may thus write $E_{ur} = 2\,(1 + \nu_{ur})\,G_{ur}$, where G_{ur} is an elastic shear modulus. In contrast to E_{ur}, the secant modulus E_{50} is not used within a concept of elasticity. As a consequence, there is no simple conversion from E_{50} to G_{50}. In contrast to elasticity based models, the elasto-plastic Hardening-Soil model does not involve a fixed relationship between the (drained) triaxial stiffness E_{50} and the oedometer stiffness E_{oed}. Instead, these stiffnesses must be given independently. To define the oedometer stiffness we use

$$E_{oed} = E_{oed}^{ref} \left(\frac{\sigma_1 + c\cot\varphi_p}{\sigma^{ref} + c\cot\varphi_p} \right)^m \quad , \tag{37}$$

where E_{oed} is a tangent stiffness modulus for primary loading. Hence, E_{oed}^{ref} is a tangent stiffness at a vertical stress of $\sigma_1 = \sigma^{ref}$.

5.2 *Advanced parameters*

Realistic values of ν_{ur} are about 0.2. In contrast to the Mohr-Coulomb model, K_0^{NC} is not simply a function of Poisson's ratio, but a proper input parameter. As a default setting one can use the highly realistic correlation $K_0^{NC} = 1 - \sin\varphi_p$. However, one has the possibility to select different values. All possible different input values for K_0^{NC} cannot be accommodated for. Depending on other parameters, such as E_{50}, E_{oed}, E_{ur} and ν_{ur}, there happens to be a lower bound on K_0^{NC}. The reason for this situation will be explained in the next section.

5.3 *Dilatancy cut-off*

After extensive shearing, dilating materials arrive in a state of critical density where dilatancy has come to an end. This phenomenon of soil behaviour is included in the Hardening-Soil model by means of a *dilatancy cut-off*. In order to specify this behaviour, the initial void ratio, e_0, and the maximum void ratio, e_{cv}, of the material are entered. As soon as the volume change results in a state of maximum void, the mobilized dilatancy angle, ψ_m, is automatically set back to zero, as indicated in Eq. 38 and Fig. 4:

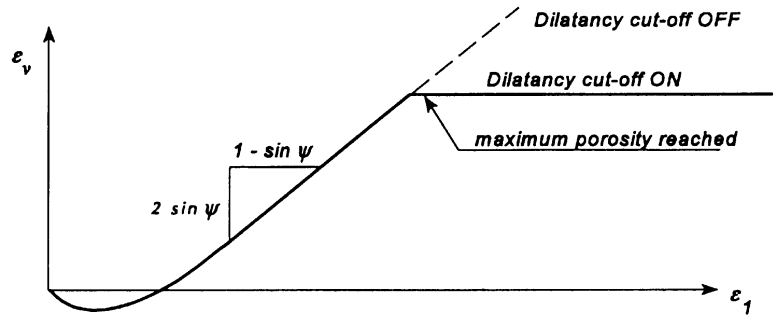

Figure 4. Resulting strain curve for a standard drained triaxial test including dilatancy cut-off.

$$\text{for} \quad e < e_{cv} \quad \sin\psi_m = \frac{\sin\varphi_m - \sin\varphi_{cv}}{1 - \sin\varphi_m \sin\varphi_{cv}} \quad ,$$
$$\text{for} \quad e \geq e_{cv} \quad \sin\psi_m = 0 \quad . \tag{38}$$

The void ratio is related to the volumetric strain, ε_v by the relationship:

$$\varepsilon_{v0} - \varepsilon_v = \ln\left(\frac{1+e}{1+e_0}\right) \quad . \tag{39}$$

where an increment of ε_v is negative for dilatancy. The initial void ratio, e_0, is the in-situ void ratio of the soil body. The maximum void ratio, e_{cv}, is the void ratio of the material in a state of critical void (critical state).

6 CALIBRATION OF THE MODEL

In a first step the Hardening-Soil model was calibrated for a sand by back-calculating both triaxial compression and oedometer tests. Parameters for the loosely packed Hostun-sand (e_0 = 0.89), a well known granular soil in geotechnical research, are given in Tab. 1. Figs. 5 and 6 show the satisfying comparison between the experimental (three different tests) and the numerical result. For the oedometer tests the numerical results consider the unloading loop at the maximum vertical load only.

7 VERIFICATION OF THE MODEL

7.1 *Undrained behaviour of loose Hostun-sand*

In order to verify the model in a first step two different triaxial compression tests on loose Hostun-sand under undrained conditions (Djedid 1986) were simulated using the identical parameter from the former calibration. The results of this comparison are displayed in Figs. 7 and 8.

In Fig. 7 we can see that for two different confining pressures of σ_c = 300 and 600 kPa the stress paths in p-q-space coincide very well. For deviatoric loads of q ≈ 300 kPa excess porewater pressures tend to be overestimated by the calculations.

Additionally in Fig. 8 the stress-strain-behaviour is compared in more detail. This diagram contains two different sets of curves. The first set (•, ♠) relates to the axial strain ε_1 at the horizontal

Table 1. Parameters of loose Hostun-sand.

ν_{ur}	m	φ_p	ψ_p	E_s^{ref} / E_{50}^{ref}	$E_{ur}^{ref} / E_{50}^{ref}$	E_{50}^{ref}
0.20	0.65	34°	0°	0.8	3.0	20 MPa

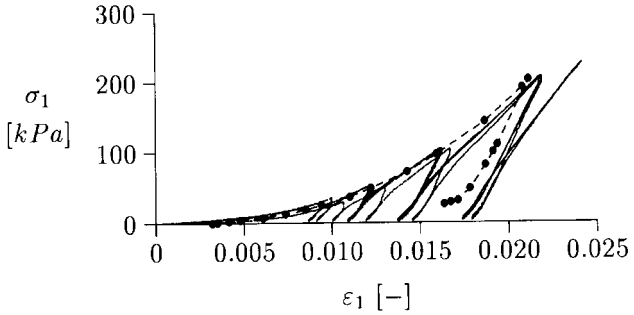

Figure 5. Comparison between the numerical (•) and experimental results for the oedometer tests.

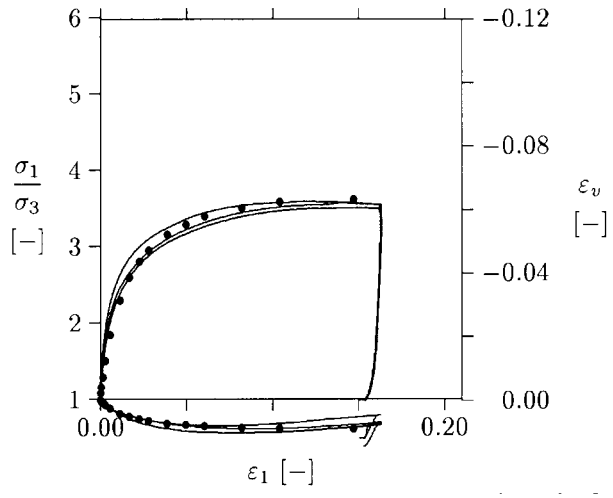

Figure 6. Comparison between the numerical (•) and experimental results for the drained triaxial tests (σ_3 = 300 kPa) on loose Hostun-sand.

and the effective stress ratio σ_1' / σ_3' on the vertical (left) axis. The second set (o, ✧) refers to the normalised excess pore water pressure $\Delta u/\sigma_c$ on the right vertical axis. Experimental results for both confining stresses are marked by symbols, numerical results by straight and dotted lines.

Analysing the amount of effective shear strength it can be seen that the maximum calculated stress ratio falls inside the range of values from the experiments. The variation of effective friction from both tests is from 33.8 to 35.4 degrees compared to an input value of 34 degrees. Axial stiffness for a range of vertical strain of $\varepsilon_1 < 0.05$ seems to be slightly over-predicted by the model. Differences become more pronounced for the comparison of excess pore water pressure generation.

Here the calculated maximum amount of Δu is higher then the measured values. The rate of decrease in Δu for larger vertical strain falls in the range of the experimental data.

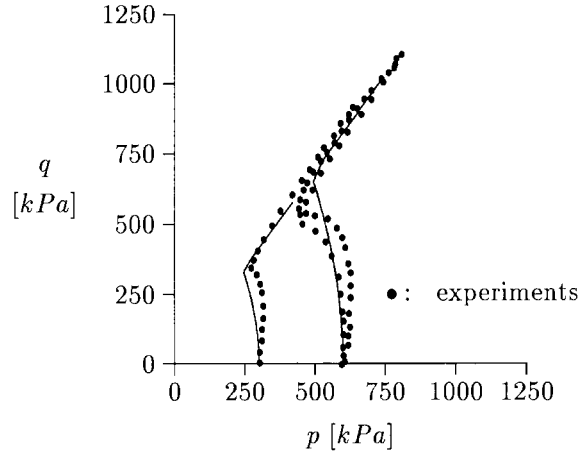

Figure 7. Undrained behaviour of loose Hostun-sand: p-q-plane.

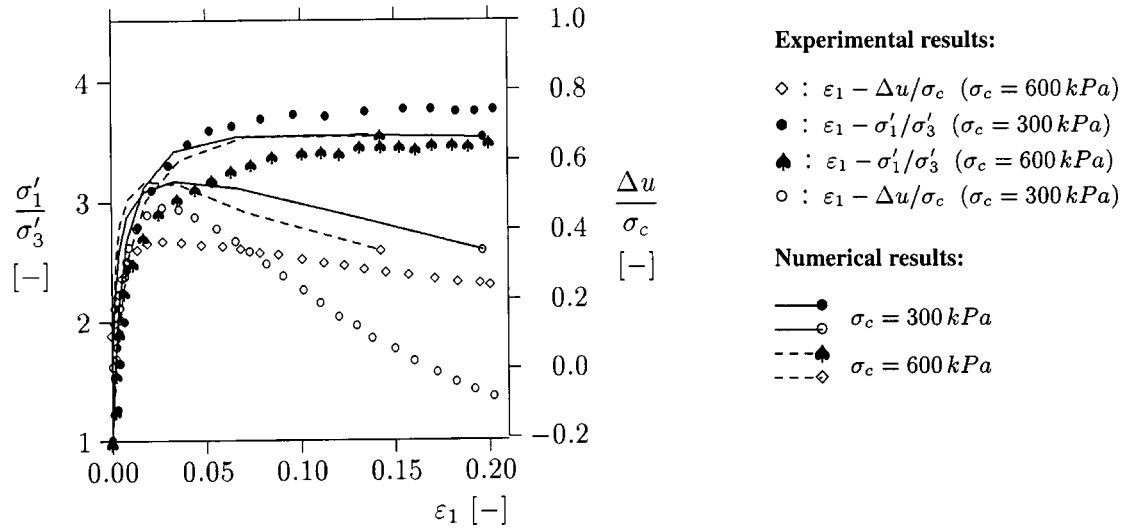

Figure 8. Undrained behaviour of loose Hostun-sand: stress-strain relations.

7.2 *Pressuremeter test Grenoble*

The second example to verify the Hardening-Soil model is a back-calculation of a pressuremeter test on loose Hostun-sand. This test is part of an experimental study using the calibration chamber at the IMG in Grenoble (Branque 1997). This experimental testing facility is shown in Fig. 9.

The cylindrical calibration chamber has a height of 150 cm and a diameter of 120 cm. In the test considered in the following a vertical surcharge of 500 kPa is applied at the top of the soil mass by a membrane. Because of the radial deformation constraint the state of stress can be interpreted in this phase as under oedometer conditions. Inside the chamber a pressuremeter sonde of a radius r_0 of 2.75 cm and a length of 16 cm is placed. For the test considered in the following example there was loose Hostun-sand ($D_r \approx 0.5$) of a density according to the material parameters as shown in Tab. 1 placed around the pressuremeter by pluviation. After the installation of the device and the filling of the chamber the pressure is increased and the resulting volume change is registered.

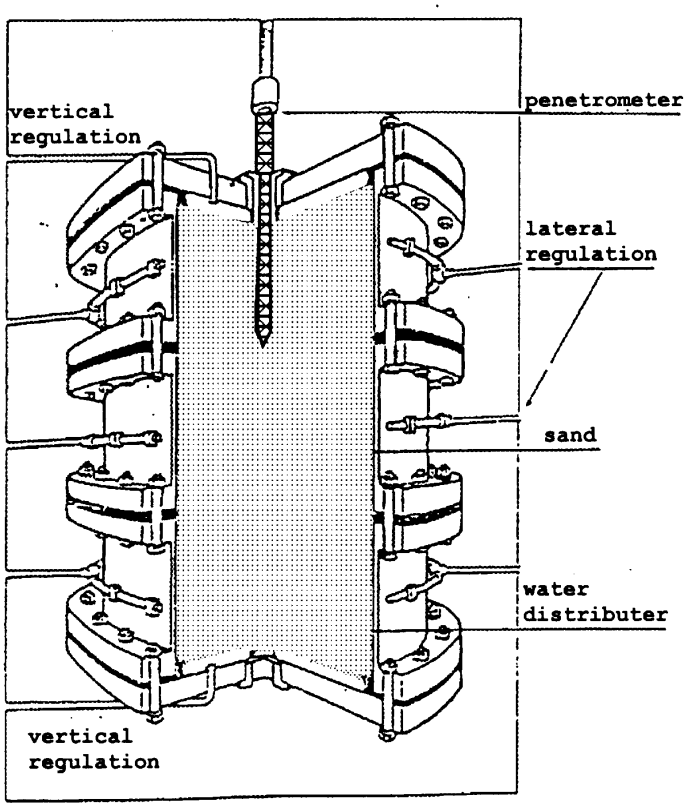

Figure 9. Pressuremeter *Grenoble*.

This experimental setup was modeled within a FE-simulation as shown in Fig. 10. On the left hand side the axis-symmetric mesh and its boundary conditions is displayed. The dimensions are those of the complete calibration chamber. In the left bottom corner of the geometry the mesh is finer because there the pressuremeter is modeled.

In the first calculation phase the vertical surcharge load *A* is applied. At the same time the horizontal load *B* is increased the way practically no deformations occur at the free deformation boundary in the left bottom corner. In the second phase the load group *A* is kept constant and the load group *B* is increased according to the loading history in the experiment. The (horizontal) deformations are analysed over the total height of the free boundary. In order to (partly) get rid of the deformation constrains at the top of this boundary, marked point *A* in the detail on the right hand side of Fig. 10 two interfaces were placed crossing each other in point *A*. Fig. 11 shows the comparison of the experimental and numerical results for the test with a vertical surcharge of 500 kPa.

On the vertical axis the pressure (relating to load group *B*) is given and on the horizontal axis the volumetric deformation of the pressuremeter. Because the calculation was run taking into account large deformations (*updated mesh analysis*) the pressure *p* in the pressuremeter has to be calculated from load multiplier Σ*Load B* according to Eq. 40, taking into account the mean radial deformation Δ*r* of the free boundary:

$$p = \Sigma LoadB \cdot \frac{r_0}{r_0 + \Delta r} \quad . \tag{40}$$

The agreement between the experimental and the numerical data is very good, both for the initial part of phase 2 and for larger deformations of up to 30%.

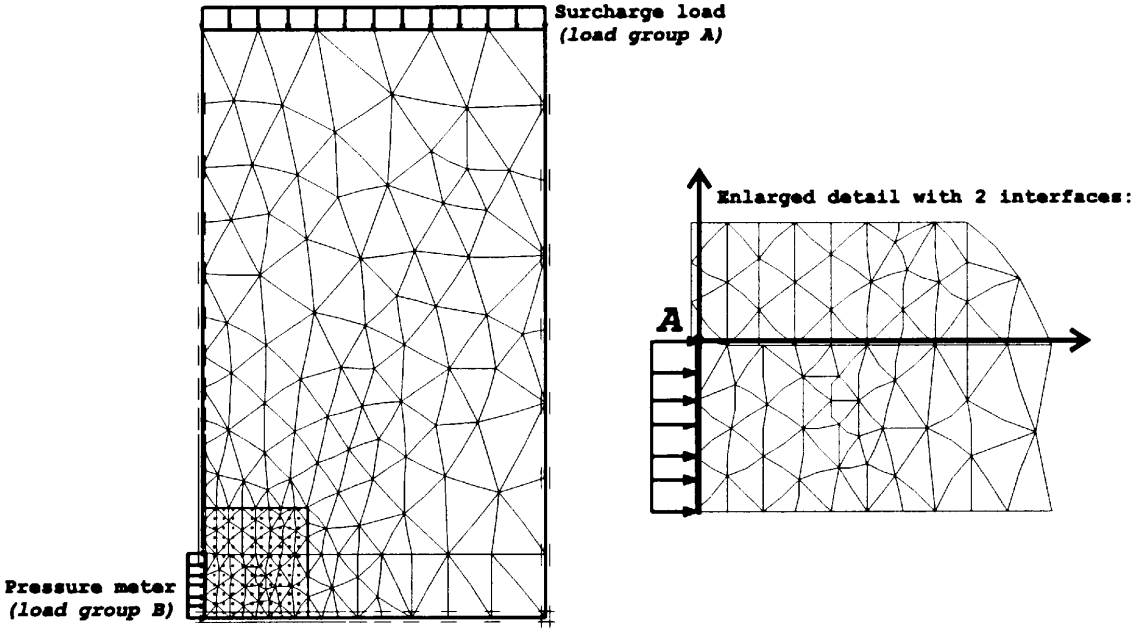

Figure 10. FE-discretization of the calibration chamber as used in the calculation.

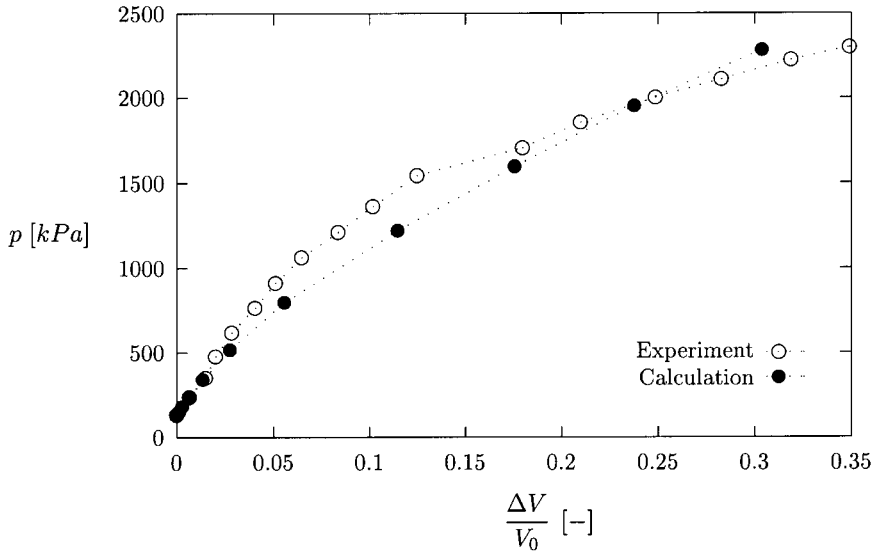

Figure 11. Comparison between experimental and numerical results of the pressuremeter test.

8 CONCLUDING REMARKS

A new constitutive model was introduced which is formulated in the framework of hardening multi-surface plasticity. The model was described in the essential equations as the ones for the yield- and plastic potential surfaces and the applied hardening laws.

After implementation of the model in the PLAXIS code it was calibrated for a loose sand using both oedometer and drained triaxial test data. With this unique set of parameters undrained shear tests and a pressuremeter test run in a calibration chamber were numerically simulated. For both verifications of the model the comparison between experimental and numerical is very promising: main characteristics of hardening soil behaviour can be described both in a qualitative and quantitative way. Because of the used set of input parameters, all parameters have a clear geotechnical relevance, the model is very attractive for the use in daily geotechnical practise.

Further developments include an extensions of database in the field of stiffness parameters for cohesive soils, the application of the model for boundary value problems in which a small strain stiffness is relevant and the 3-dimensional verification of the model.

REFERENCES

Branque, D. (1997), Utilisation d'un modèle Élasto-plastique avec dilatance dans I'interprétation de l'essai pressiométrique sur sable, PhD thesis, Ecole Centrale Paris.

Djedid, A. (1986), Etude du comportement non-drainé du sable, Mémoire de D.E.A., Institut de Mécanique de Grenoble.

Duncan, J.M. & Chang, C.Y (1970), Nonlinear analysis of stress and strain in soil, *J. Soil Mech. Found. Div. ASCE* 96, 1629-1653.

Hashiguchi, K. (1985), Macrometric approaches-static-instrinsically time-independent, *in* Proc. XI ICSMFE, San Francisco, Constitutive laws for soils, pp. 25-65.

Hashiguchi, K. (1993), Fundamental requirements and formulations of elastoplastic constitutive equations with tangential plasticity, *Int. J. Plasticity* 9, 525-549.

Koiter, W.T. (1960), General theorems for elastic-plastic solids, *in* Sneddon & Hill, eds, Progress in Solid Mechanics, North Holland Publishing Co., Amsterdam, pp. 165-221.

Kondner, R.L. & Zelasko, J.S. (1963), A hyperbolic stress strain formulation for sands, *Proc.* 2nd *Pan. Am. ICOSFE Brazil* 1, 289-394.

Rowe, P.W. (1962), The stress-dilatancy relation for static equilibrium of an assembly of particles in contact, *Proc. Roy. Soc.* A. 269, 500-527.

Rowe, P.W. (1971), Theoretical meaning and observed values of deformation parameters for soil, *in* Proc. of Roscoe memorial symposium, Foulis, Henley-on-Thames, pp. 143-194.

Schanz, T. & Vermeer, P.A. (1996), Angles of friction and dilatancy of sand, *Géotechnique* 46, No. 1, 145-151.

Schanz, T. & Vermeer, P.A. (1998), On the stiffness of sands, *Géotechnique* 48, 383-387.

Vermeer, P.A. & Brinkgreve, R.B.J. (1998), PLAXIS: Finite element code for soil and rock analyses (Version 7.l), B alkema, Rotterdam.